Open Orbits and the Fermi Surface of Gallium by an Induced-Torque Method

J. R. Cook and W. R. Datars*
Department of Physics, McMaster University, Hamilton, Ontario, Canada
(Received 14 August 1969)

An investigation of the open-orbit structure in gallium at 1.4°K using the induced-torque technique has yielded direct information on the connectivity of the sixth-band hole surface. This surface supports a k_c trajectory for all field directions in the *ab* plane, except within 0.1° of the *a* axis. A smaller-amplitude k_a trajectory is reported, existing over a 10° range of field direction centered (32±2)° from the *b* axis in the *bc* plane. These data, in addition to the highly anisotropic amplitude and field dependence of the k_c trajectory, require that this surface contact the Brillouin-zone boundary at both the k_a and the k_c faces. The present data are compared with available models of the sixth-band hole surface and are found to be in excellent agreement with the predictions of Reed's pseudopotential calculations. The possibility of magnetic breakdown in the k_c trajectory for $\mathbf{B}\|$ (*b* axis) is discussed. Finally, a nonlinear frequency dependence, and an anisotropic, nonquadratic field dependence of the induced torque are understood to occur through the long mean free path and short skin-depth parameters in gallium at 1.4°K.

I. INTRODUCTION

GALLIUM is a compensated metal that characteristically supports a complicated Fermi surface comprised of many separate sheets, some of which are very complex. Although there exists a large body of experimental data, including magnetoresistance,[1] de Haas–van Alphen,[2,3] rf size effect,[4,5] magnetoacoustic effect,[6,7] cyclotron resonance,[8] dc size effect,[9] and others,[10] the Fermi surface in some of these bands was not well established. The essential complexity of these surfaces, further complicated by the effects of magnetic breakdown[2,8,10] and the approximations involved in the Fermi-surface-model calculations, usually made comparison of theoretical and experimental work difficult. Attempts have been made to compare these data with the single-orthogonalized-plane-wave (OPW)[1,11] and with the preliminary augmented-plane-wave (APW) calculations.[2,12] While approximate agreement was obtained for most surfaces, the largest discrepancy was the topology of the sixth-band hole surface. This is the only surface considered capable of supporting open trajectories. In particular, the single-OPW model predicts the existence of a large number of open trajectories, while the APW model predicts the existence of a single k_a trajectory. On the other hand, the magneto-resistance data[1] indicated that only k_c trajectories exist. The present detailed study of the open-orbit structure in gallium was undertaken in an attempt to resolve these discrepancies and to elucidate the connectivity of the sixth-band hole surface.[13] At a late stage in this investigation, the pseudopotential calculations of Reed[14] become available for comparison with present data. This calculation indicates a sixth-band topology deviating widely from that of either the single-OPW or APW approximations. This model possesses connectivity in both the k_a and the k_c directions; this connectivity supports both k_a and k_c open trajectories over discrete ranges of magnetic field direction.

The induced-torque technique[15] was used for several reasons. This method has the distinct technical advantage of requiring no electrical connections to a sample, the volume and geometry of which are widely variable. In addition, solid-angle data are obtainable and are particularly valuable for a spherical sample. Beyond these immediate experimental advantages, this method was chosen in an attempt to extend and refine the technique. This aim was particularly feasible with the long mean free path and low residual resistivity obtainable in gallium.

II. THEORY

The induced-torque technique depends on the variations in retarding torque exerted by a sample suspended from the movement of a nulling galvanometer as a magnetic field **B** is slowly rotated in a horizontal plane.[15] The vector quantities involved are shown in Fig. 1: A primed coordinate reference frame is established rotating about a fixed y' axis at a low angular velocity ω, in synchronism with the magnetic-field-defined z' axis; a second coordinate frame rotates with the z axis defined along the z' axis, with the y axis defined at a fixed *tilt angle* β from the vertical y' direction. The rotating magnetic field induces current in the stationary sample creating a magnetization **m** which couples with the

* E. W. R. Steacie Research Fellow.
[1] W. A. Reed and J. A. Marcus, Phys. Rev. **126**, 1298 (1962).
[2] A. Goldstein and S. Foner, Phys. Rev. **146**, 442 (1966).
[3] J. M. Condon, Bull. Am. Phys. Soc. **9**, 239 (1964).
[4] J. F. Cochran and C. A. Shiffman, Phys. Rev. **140**, A1678 (1965).
[5] A. Fukumoto and M. W. P. Strandberg, Phys. Rev. **155**, 685 (1967).
[6] Y. Shapira and B. Lax, Phys. Rev. **138**, 1191 (1965).
[7] L. J. Neuringer and Y. Shapira, Phys. Rev. **165**, 751 (1960).
[8] T. W. Moore, Phys. Rev. **165**, 864 (1967); Phys. Rev. Letters **18**, 310 (1967).
[9] M. Yaqub and J. F. Cochran, Phys. Rev. **137**, A1182 (1965).
[10] J. A. Munarin, Phys. Rev. **172**, 737 (1968).
[11] J. C. Slater, G. F. Koster, and J. H. Wood, Phys. Rev. **126**, 1307 (1962).
[12] J. H. Wood, Phys. Rev. **146**, 432 (1966).
[13] J. R. Cook and W. R. Datars, in *Proceedings of the Eleventh International Conference on Low Temperature Physics*, edited by J. F. Allen, D. M. Funlayson, and D. M. McCall (University of St. Andrews Printing Department, St. Andrews, Scotland, 1969).
[14] W. A. Reed, Phys. Rev. **188**, 1184 (1969).
[15] J. S. Moss and W. R. Datars, Phys. Letters **24A**, 630 (1967).

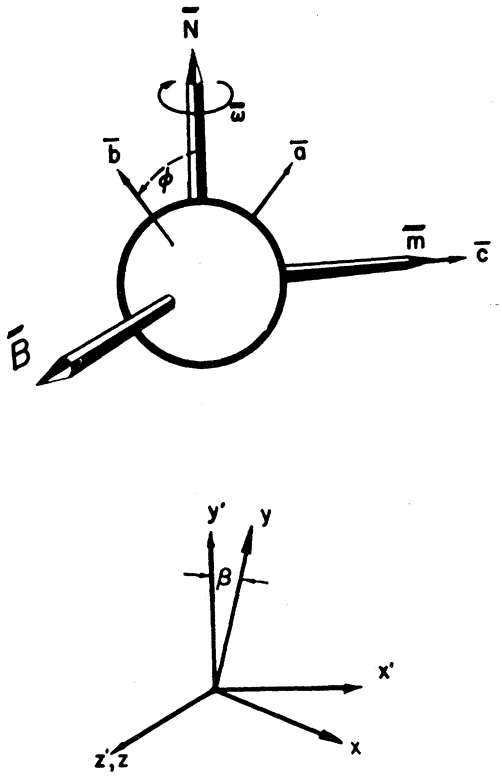

FIG. 1. Vector quantities and coordinate systems used in the induced-torque problem.

inducing field to produce a torque **N**. Only the y' component ($N_{y'}$) of this torque is monitored by the apparatus.

The currents induced in the sample flow in accordance with the boundary conditions and the conductivity components $\sigma_{\nu\mu}$ which are, in general, anisotropic. The components of $\sigma_{\nu\mu}$ govern the galvanomagnetic response of the metal, and are defined in the high-field limit ($\omega_c\bar{\tau}\gg1$) through integrals over the Fermi surface. The observed induced-torque amplitude experiences a sharp increase as the form of the conductivity matrix alters with the occurrence of an open trajectory in the plane orthogonal to **B**. The problem is to relate the observable torque to the particular components of $\sigma_{\nu\mu}$ from which may be inferred the geometric features of the Fermi surface.[16–18] Although a rigorous solution for the case of an anisotropic conductivity has not been obtained, an approximate solution based on a simplified model, assuming a localized and steady-state current distribution, has been presented.[19] The basis of this model is the essential unidirectional character of a band of open trajectories which tends to confine induced current in the plane of high conductivity normal to the open-orbit direction in the high-field limit.[16–18] If this direction, defined by the x axis in Fig. 1, is tilted out of the magnet sweep plane, the yz plane of high conductivity tips accordingly, introducing dependences in tilt angle β to Eq. (7) of Ref. 19. It is a natural consequence that the longitudinal magnetoresistance ($\rho_{zz}=\rho_{z'z'}$) component is not altered by tipping, but that the effective transverse magnetoresistance ($\rho_{y'y'}=\rho_{yy}/\cos\beta$) increases. In this model calculation, the induced torque per unit volume becomes, for spherical samples of radius a,

$$N_{y'}=\omega a^2B^2\sigma^*/10c^2, \tag{1}$$

where

$$\sigma^*=2\cos\beta/(\rho_{yy/\cos\beta}+\rho_{zz})$$
$$=\frac{2\cos^2\beta\,\mathrm{Det}}{\sigma_{xx}\sigma_{zz}+\sigma_{xz}^2+(\sigma_{xx}\sigma_{yy}+\sigma_{xy}^2)\cos\beta}, \tag{2}$$

where c is the velocity of light and σ^* is a reduced conductivity.[20,21] The extrinsic quadratic field dependence of Eq. (1) is modulated by the functional form of σ^* with its intrinsic field dependence. This modulation is most pronounced if magnetic breakdown occurs,[19] but is also influenced by the long mean free path in gallium. The linear frequency dependence is a direct consequence of the assumption that the skin depth is substantially larger than the sample dimensions ($\delta\gg a$).

III. EXPERIMENTAL

The induced-torque magnetometer[15] consists of an electronic nulling galvanometer sensitive to the small torques generated in a sample suspended in a rotating magnetic field. The basic galvanometer is of the design of Condon and Marcus,[22] as modified by Vanderkooy and Datars.[23] An inherent feature of this apparatus is that the sample orientation may be changed during the course of an experiment by rotation about a fixed, nominally horizontal axis in order to study any crystallographic plane containing this axis. It is often desirable to align an open trajectory along this fixed axis, allowing **B** to intersect the plane orthogonal to this direction. The induced-torque investigations in gallium used the apparatus constructed by Moss.[15] Slotted sample holders are pinned into a drum, which is rotated about a horizontal axis by means of a worm gear. In use, this assembly is suspended from the galvanometer movement by a quartz rod but may be raised from this connection to allow the worm gear to contact a shaft. This shaft, rotated from above the Dewar, is used to rotate the drum in increments as small as $\frac{1}{12}°$. The usual increment, however, was 1°.

[16] I. M. Lifshitz, M. I. Azbel and M. I. Kagonov, Zh Eksperim. i Teor. Fiz. **31**, 63 (1956) [English transl.: Soviet Phys.—JETP **4**, 41 (1957)].
[17] I. M. Lifshitz and V. G. Peschanskii, Zh. Eksperim. i Teor. Fiz. **35**, 1251 (1958); **38**, 188 (1960) [English transls.: Soviet Phys.—JETP **8**, 875 (1959); **11**, 137 (1960)].
[18] E. Fawcett, Advan. Phys. **13**, 139 (1964).
[19] W. R. Datars and J. R. Cook, Phys. Rev. **187**, 769 (1969).
[20] For cylindrical samples of radius a, the torque per unit volume is $N_{y'}=(\omega a^2B^2/8c^2)\sigma^*$.
[21] J. R. Cook, thesis, McMaster University (unpublished).
[22] J. H. Condon and J. A. Marcus, Phys. Rev. **134**, A446 (1964).
[23] J. Vanderkooy and W. R. Datars, Phys. Rev. **156**, 671 (1967).

An important consideration is the alignment of the drum axis with the magnet sweep plane and with a nominally aligned crystal axis. The former angle is controlled by precision machining and by ensuring that the support axis is precisely vertical. The rotating magnet was found by autocollimation techniques to sweep a horizontal plane within 20′ of arc. The uncertainty of alignment of the drum rotation axis is approximately 2°, and is defined as the angle ζ. The angle between the drum axis and the crystal axis nominally aligned collinear with the sample holder is defined as ξ. The angle is composed of two contributions: small errors in alignment of the crystal using the Laue technique and slight misalignments intrinsic in placing the sample holder in the drum rotator. The total angle ξ is approximately 2°.

As the drum is rotated, ostensibly presenting the same oriented crystal axis to the magnet sweep plane. this axis describes an approximate arc about the drum axis. If $\xi>\zeta$, there occur two regions of angle in a complete drum rotation over which the crystalline axis will be very closely aligned in the magnet sweep plane. Although the nominal crystal alignment is 1° by x-ray techniques, the actual alignment to a specific crystalline axis may be brought to better than 0.1° by using this wobble intrinsic in the apparatus. This technique is extremely useful in studies requiring very accurate alignment.

The entire assembly, in a Dewar system suspended between the pole tips of a rotating electromagnet, was maintained at 1.4°K by pumped liquid helium. Angular rotation speeds of the electromagnet could be set between 5°/min and 60°/min; field intensities up to 20 kOe were used. Rotation data were taken at constant field and rotation frequency.

The samples used in this investigation were grown in sample holders in two basic shapes from 99.999 99%-purity gallium supplied by Eagle Picher. Cylindrical samples, nominally 0.275 in. in diam by 0.70 in. in length were grown in machined Kel-F holders. Spherical crystals were grown in the cavity formed by the removal of a 0.205-in.-diam ball bearing encapsulated in RTV615 silicon potting material. The holder in each case was filled with gallium and the entire assembly raised above the transition temperature 29.78°C.[5] An oriented seed at room temperature was contacted to the melt, and partially melted to ensure intimate contact. The melted contacting region was then stretched to a filament to reduce the area of thermal contact and hence decrease the crystal growth rate. The assembly was allowed to cool to room temperature, the actual crystal growth requiring about 20 min. The seed was detached with a hot wire, and the orientation checked by Laue techniques.

An example of rotation data obtained for a 11-kOe magnetic field, with a rotation speed of 47°/min is shown in Fig. 2 for the two senses of rotation. The large peak appearing at 0° is due to the k_c open-orbit trajectory previously reported.[1] The induced torque appears with identical amplitude, but opposite sign for the two directions of rotation. The de Haas–van Alphen background which is evident 40° on either side of the induced-torque peak in Fig. 2 does not so invert and may usually be separated from the induced torque. The half-width of the induced-torque peak is approximately $\frac{1}{2}$°, which is regarded as the minimum width obtainable for an unstrained crystal. With sweep speeds below 60°/min, no appreciable change in apparent width was observed which could be attributed to the 0.15-sec response time of the electronics.

IV. EXPERIMENTAL RESULTS

Shown in Fig. 3 is a composite stereographic presentation of field directions in which open orbits were observed using five different crystal orientations *A–E*. The fixed horizontal axis of the sample holder was within 1° of the *a*, *b*, and *c* crystallographic axes in orientations *A–C*, respectively. In addition, orientations 50° from the *a* axis in the *ac* plane (*D*) and 32° from the *b* axis in the *bc* plane (*E*) were used.

An essential feature of the induced-torque apparatus is that the sample orientation may be changed *in situ* by rotation about the nominally horizontal oriented axis. With an open orbit directed along this axis, the induced torque is observed with the open orbit, magnetic field, and torque observation directions mutually orthogonal ($\cos\beta=1$). A convenient measure of drum rotation is provided when symmetry directions in the crystal have been established. With a k_c open orbit directed along the fixed axis of a *C* crystal orientation, the angle θ_{ab} is defined as the direction of magnetic field in the crystal at which the open orbit is observed, measured from the *a* axis in the *ab* plane.

The induced-torque amplitude of the k_c open trajectory obtained with a spherical *C* crystal is presented in Fig. 4 as a function of θ_{ab} for five field intensities. The lack of exact mirror symmetry in amplitude about the *b* axis is due to the slight irreducible wobble discussed in Sec. III; however, the mirror symmetry of all important features is retained. The observed amplitude at a particular field intensity is relatively constant for $16°<\theta_{ab}<56°$, but is heavily structured for larger angles, exhibiting three distinct peaks, and a narrow minimum at $(68-61)°$, $(70.5\pm1)°$, $(76.6\pm1)°$, and $(74.0\pm1)°$, respectively. The first peak shifts linearly from $(68\pm1)°$ to $(61\pm1)°$ as the field intensity is increased from 2 to 19 kOe. The field dependence is seen from this graph to be approximately linear for $\theta_{ab}<56°$, with a sudden change in character for $\theta_{ab}>56°$. Figure 5 presents a log-log plot of induced-torque amplitude as a function of field intensity for several values of θ_{ab}. The dependence is found to be generally between quadratic and linear, but changing with angle, and in the instance of the $(68-61)°$ peak, with field intensity.

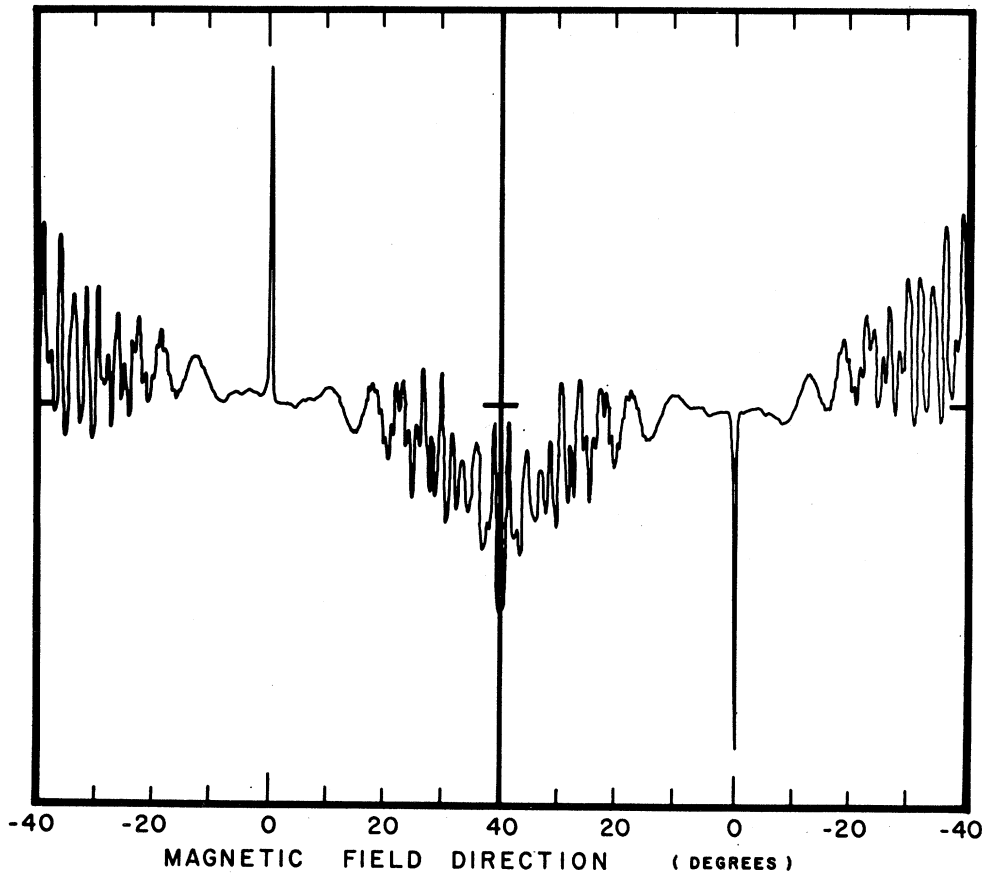

FIG. 2. Torque obtained from a spherical, C-axis crystal of gallium at $\theta_{ab}=63°$, for a field intensity of 11 kOe and a rotational speed of 47°/min, for rotations from −40° to 40° and from 40° to −40°.

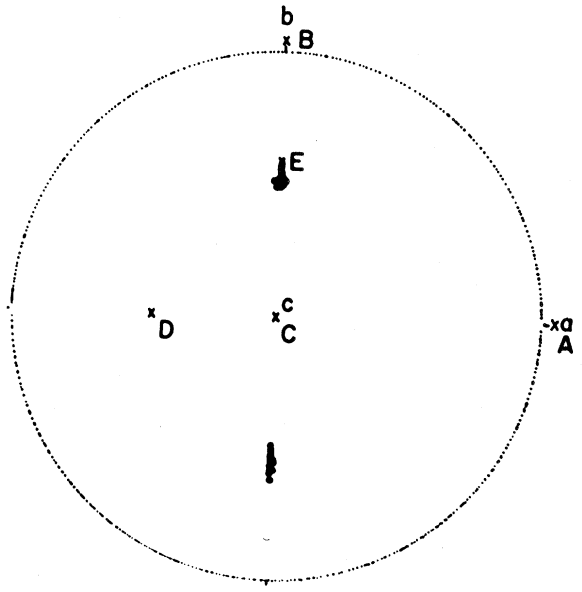

FIG. 3. Composite stereogram of magnetic-field directions in which open orbits in gallium were observed by induced torque. A–E indicate the orientations of the five samples.

The dependence of torque amplitude on tilt angle β was observed using a cylindrical B crystal; the k_c trajectory is observed at the b axis for all tilt angles, except when the c axis and torque observation directions are collinear ($\theta_{ca}=\beta=\frac{1}{2}\pi$). The observed tilt dependence exhibits a smooth geometric dependence, as shown in Fig. 6 for 8 kOe with $\omega=30°$/min.

The induced-torque amplitude due to the k_c trajectory exhibits a broad null of 13° half-width centered at the a axis. With a cylindrical A crystal, the angular width of absolute null has been determined using the intrinsic wobble of the apparatus by monitoring the induced-torque amplitude due to the k_c trajectory as a function of tilt angle β. The general geometric dependence illustrated in Fig. 7 as a function of rotation angle ($\theta_{cb}=\beta$) is strongly modulated by the amplitude variation occurring as **B** sweeps near the a-axis null. The dip at the b axis occurs as the k_c trajectory and torque observation directions become collinear ($\beta=\frac{1}{2}\pi$). In the region of small tilt angle, over which the observed amplitude is expected to be largest, there is a broad null centered near $\theta_{cb}=15°$. The origin of this null is the close alignment of **B** with the a axis. It is concluded

from these data that the a axis is an absolute null, to the sensitivity of the apparatus, in an angular width of 0.1°; the k_c trajectory does not exist for **B** within 0.1° of the a axis. On the stereogram (Fig. 3) the observation directions in the ab plane appear as a continuous series of points on the periphery, excluding the a axis.

A second open trajectory has been found, existing over a 10° range of field direction centered (32±2)° from the b axis in the bc plane.[13] This group exists for only a small (3°) angular range out of the plane, as shown on the stereogram in two equivalent regions of the bc plane. The maximum amplitude of this group is relatively small (2%) compared with the maximum amplitude of the k_c group. This small amplitude, and the observed field dependence suggest that the corresponding magnetoresistance remains nonsaturating. In a 360° drum rotation using a cylindrical A crystal, this group is observed over four regions equivalent by symmetry as shown in Fig. 8. The variations in amplitude and the apparent anisotropy are a direct consequence of the irreducible wobble of the apparatus. This variation indicates a rapidly altering Fermi-surface topology. A second orientation is required to uniquely define the direction of this second group. Using an E crystal in a tilt dependence plot similar to Fig. 6, the maximum appears with the a axis horizontal. The second group is, therefore, defined to be a k_a trajectory. Supporting evidence is the inability to observe this group with a

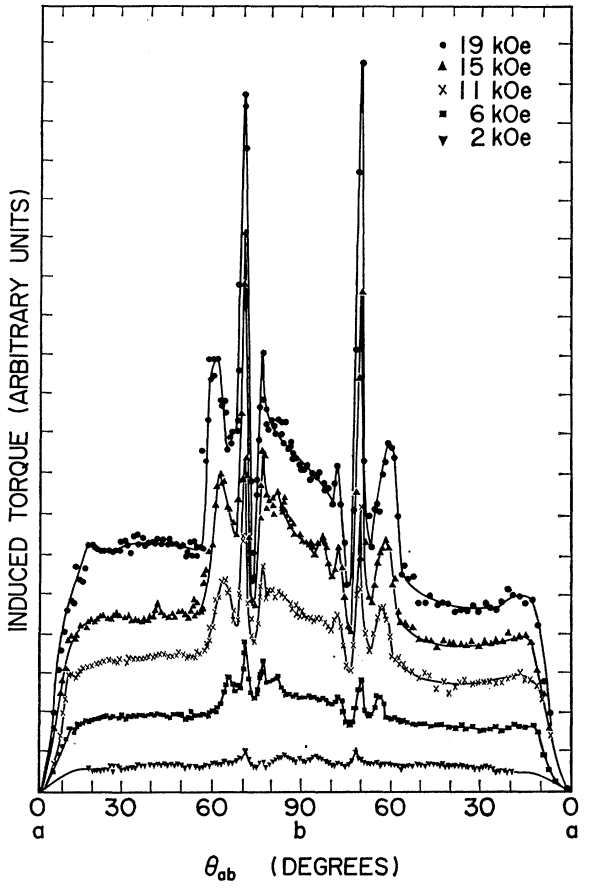

FIG. 4. Induced-torque amplitude of the k_c trajectory observed in the ab plane for five values of field intensity (2, 6, 11, 15, and 19 kOe), at a magnet rotation speed of 30°/min, using a spherical sample. The torque, open orbit, and magnetic-field directions were mutually orthogonal at each observation direction.

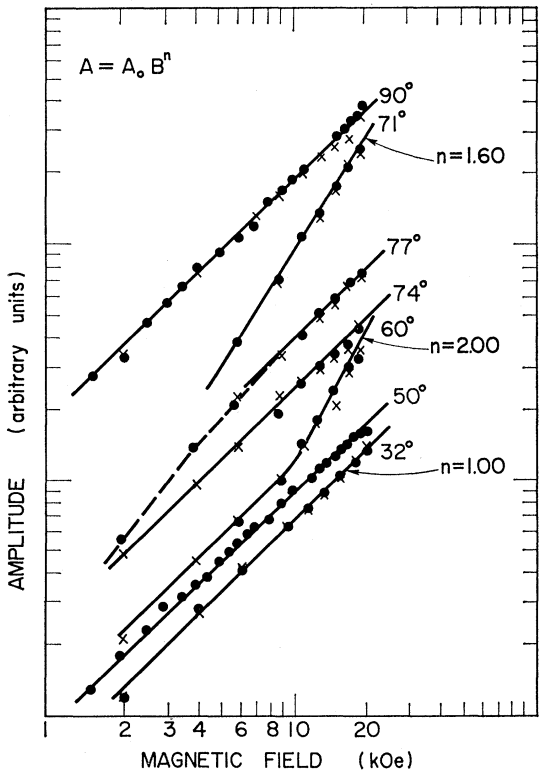

FIG. 5. Log-log plot of the dependence of the k_c trajectory on field intensity for several observation directions in the ab plane. The dependence approximates B^n for most direction ($n = 1.00 \rightarrow 2.00$).

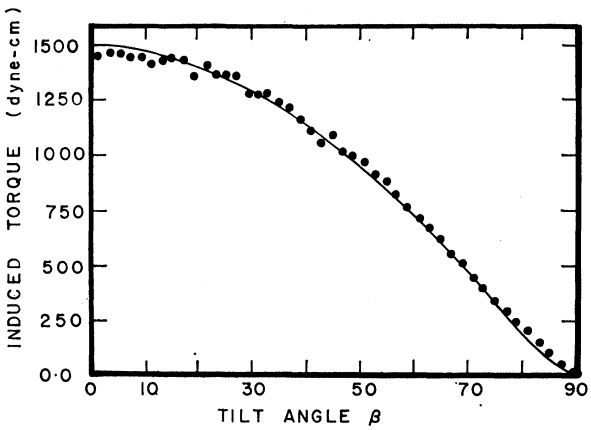

FIG. 6. Dependence of k_c trajectory induced torque on tilt angle β for 8-kOe field intensity, at a rotation speed of 30°/min with **B** parallel to the b axis.

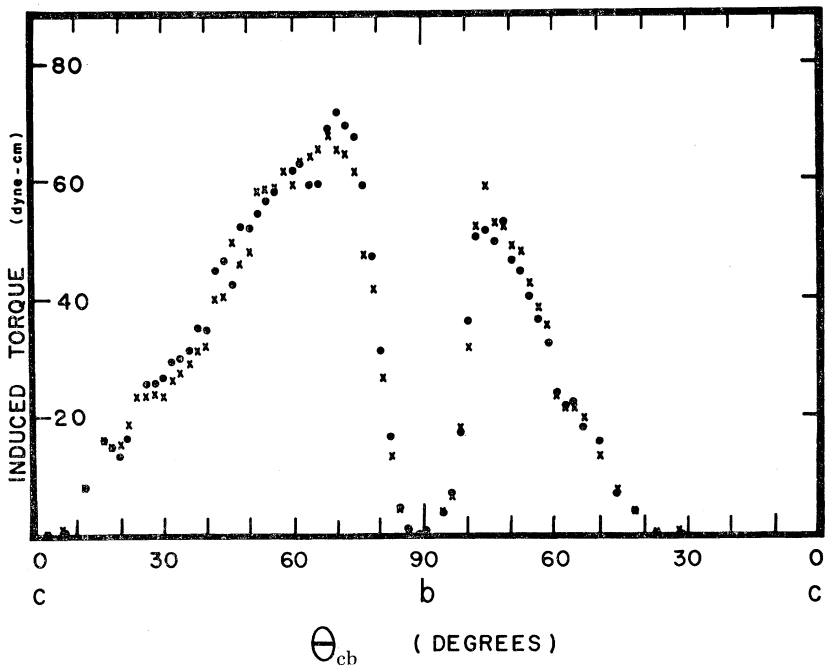

FIG. 7. Amplitude of the k_c trajectory tilt dependence with field direction near the a axis (field intensity of 5 kOe, rotation speed of 30°/min).

B crystal. This follows since a k_a trajectory would be collinear with the vertical axis ($\beta=\frac{1}{2}\pi$) when $\mathbf{B}$ is orthogonal to it, and hence unobservable.

A recorder trace of the two open-orbit peaks observed at $\theta_{bc}=32°$ using an A crystal is shown in Fig. 9, for a single magnet sweep θ over 90° at 8 kOe, with $\omega=30°/\text{min}$. The superimposed vector diagram indicates the geometric arrangement and demonstrates that the open-orbit peak due to the k_a open orbit appears at $\theta=90°$. Since the k_c trajectory is observed near the a-axis null, the amplitudes of the two peaks appear similar. Superimposed on the induced-torque peaks are small de Haas–van Alphen oscillations; a series of oscillations due to the mechanical motion of the system appear after the second peak.

The suggestion[10] that magnetic breakdown may occur in the k_c trajectory for $\mathbf{B}\|b$ axis was investigated using a spherical C crystal. The induced torque due to the k_c trajectory was monitored as a function of field intensity in $\frac{1}{12}°$ steps about the b axis. As shown in Fig. 5 for $\theta_{ab}=90°$, the dependence on field intensity is virtually linear below 20 kOe.

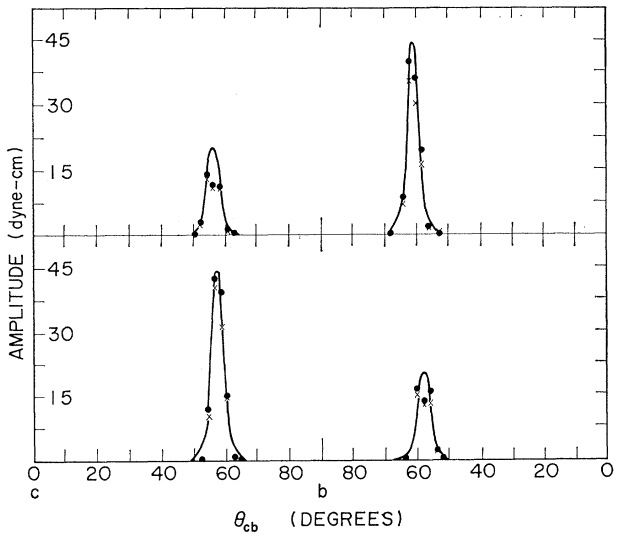

FIG. 8. Induced-torque amplitude of k_a trajectory for the magnetic-field crossing directions over 360° in the bc plane. The difference in amplitude in different quadrants is due to the slight wobble intrinsic in the apparatus.

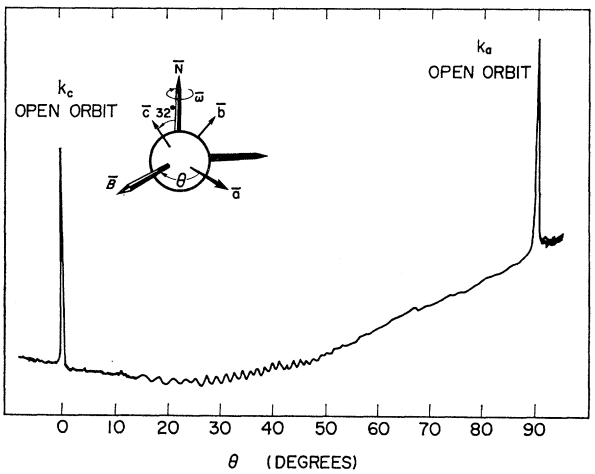

FIG. 9. Recorder tracing of simultaneous observation of the k_c and k_a trajectories. The crystal orientation is indicated by superimposed vector diagram. The k_c trajectory appears at $\theta=0°$; the k_a trajectory appears at $\theta=90°$.

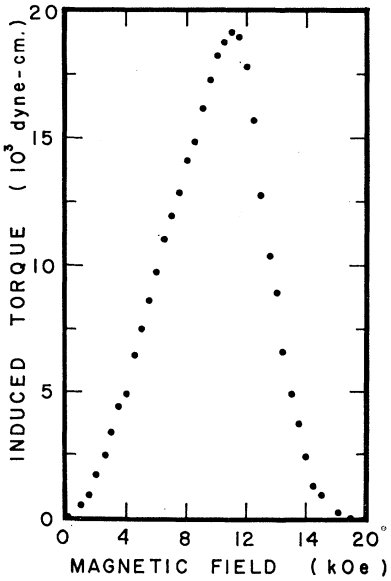

FIG. 10. Induced-torque field dependence observed with $\mathbf{B}\|b$ axis using a cylindrical crystal oriented along the b axis. The tilt angle β of the k_c trajectory is 77°; the rotational speed is 30°/min.

With a B crystal, the induced-torque amplitude was plotted as a function of tilt angle for several field intensities. The general geometric dependence observed below 10 kOe has been presented for 8 kOe in Fig. 6. At high fields over a narrow region of tilt angle, however, the amplitude is reduced in a manner which suggests the occurrence of breakdown. This reduced amplitude is found over a 1° range of coincidence between **B** and the b axis, but is more pronounced over a 0.1° range. The dependence for this range exhibits the peak value at the low field intensity of 10 kOe, and the lowest amplitude (null) at high fields, as shown in Fig. 10. Obtained at large tilt angle (77°), these induced-torque peaks were observed to split into two separate peaks in addition to decreasing at higher field intensities.

The dependence of induced-torque amplitude on magnet rotation frequency for 5 kOe, at 1.4°K, for both the k_a and k_c trajectories using the A crystal is presented in Fig. 11.

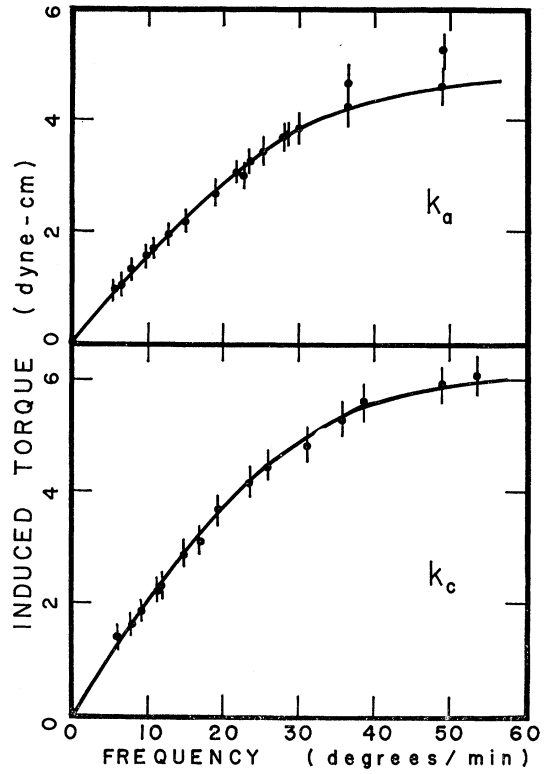

FIG. 11. Frequency dependences of k_a and- k_c-induced torque with computed fits.

V. DISCUSSION

The assumption in the derivation of Eqs. (1) and (2) is that the mean free path Λ is small compared with the typical sample dimensions a, or with the distances over which the fields in the crystal are varying appreciably. The latter is characterized by the skin-depth parameter over the accessible frequency range (2.3×10^{-4}–2.8×10^{-3} Hz). Using an appropriate value[9] of bulk resistivity at 1.4°K, $\rho_0=5.5\times10^{-23}$ esu, $\delta\cong1.69$–4.87 cm. Also, Λ has been determined[4,6,9,12] to be approximately 1.8 cm at 1.4°K, several times larger than the sample radius. Hence, the mean free path is appreciably larger than the sample dimensions and approximates the skin depth ($\delta>\Lambda>a$). The potential seen by the electrons diffusing in the sample volume is, therefore, spacially varying.

Thus, the initial assumption used in the derivation of Eqs. (1) and (2) is not strictly valid for gallium. The long mean free path and short skin-depth parameters will be shown in Secs. V B and V D to profoundly affect the field and frequency dependence of the observable induced torque.

A. Connectivity of Fermi Surface

The induced-torque data require a Fermi-surface topology capable of supporting two separate open-trajectory groups having net directions in the k_c and k_a directions. Further, the k_c group does not exist for field directions within 0.1° of the a axis; the k_a group exists for a restricted 10° range of field direction in the bc plane, (32±2)° from the b axis. These data place stringent constraints on the topology of proposed models of the Fermi surface.

The unmodified single-OPW model supports open trajectories for a multitude of field directions on the sixth-band hole surface[1,11]: a k_c trajectory for all field directions in the ab plane, except near the a axis; a k_a trajectory for $\theta_{bc}=0°$; a trajectory in the bc plane for

$\theta_{bc} \simeq 59°$. The observed dependence of the k_c trajectory is in approximate agreement with this model; however, of the remaining predicted trajectories only the k_a group in the vicinity of $\theta_{bc}=30°$ can be associated with present data. The *ad hoc* modification of the single-OPW model proposed by Reed and Marcus[1] to fit their magnetoresistance data eliminated all but the k_c trajectory and further modified the surface to allow the existence of this group for $\mathbf{B}\|a$ axis. This model does not possess the required connectivity.

The sixth-band hole surface calculated by the APW approximation[12] supports open trajectories only in the k_a direction for all field directions in the *bc* plane: The APW model does not possess the required restricted k_a connectivity.

Figure 12 is a representation of a deformed single-OPW model which retains the essential connectivity required by present data.[13] The vestigal neck connection is retained providing the required k_a connectivity. The only connectivity in the k_bk_c plane is at the k_c faces of the Brillouin zone $\pm(25\pm5)°$ from the k_c axis. The assumption of a small k_a-neck area at the zone face is made in consideration of the relatively small torque amplitude observed for the k_a trajectory. By virtue of the double arm connections to the k_c-zone faces, this surface supports two groups of open trajectories over a range of field directions ($56°<\theta_{ab}\leqslant 90°$). One trajectory exists for ($56°<\theta_{ab}<90°$), traversing a rapidly altering topology. The other exists for all θ_{ab} except near the *a*-axis null and when intersecting the vestigial k_a-neck connection.

A model of the gallium Fermi surface determined from the pseudopotential calculations of Reed[14] is shown in Fig. 13. The Fermi surface in the sixth band appears as two convoluted k_c-directed cylinders with four k_a-directed interconnections. This surface contacts the Brillouin-zone boundary at the center of the k_a faced and bears a remarkable resemblance to the proposed surface shown in Fig. 12, with the exception that each k_c-arm connection is doubled and exists out of the $k_a=0$ plane. In satisfactory agreement with the experimentally determined 10° range centered at $\theta_{bc}=(32\pm2)°$, the k_a trajectories traverse the k_a-neck and k_a-arm connections for magnetic fields directed 28°–34° from the *b* axis in the *bc* plane. For a general field direction in the *ab* plane, except near the *a* axis, both an inner and outer group of k_c trajectories are supported at each arm connection. No k_c trajectories are possible for $\mathbf{B}\|a$ axis, because the convoluted cylinders dip out of the k_c connectivity plane. The outer group exists for a general field direction, except when interdicted by the k_a-neck connection. This model, therefore, exhibits the correct connectivity over the approximate angular ranges observed experimentally. The protuberances in the k_bk_c plane 35° off the k_c axis reported in the rf-size effect[5] and ultrasonic-attenuation[6] experiments are identified as the k_a-arm connections. The conclusions of Shapiro and Lax,[6] and Goldstein and Foner[2] that contact occurs in the k_bk_c plane at angles larger than 13.5° from the k_c axis are also confirmed.

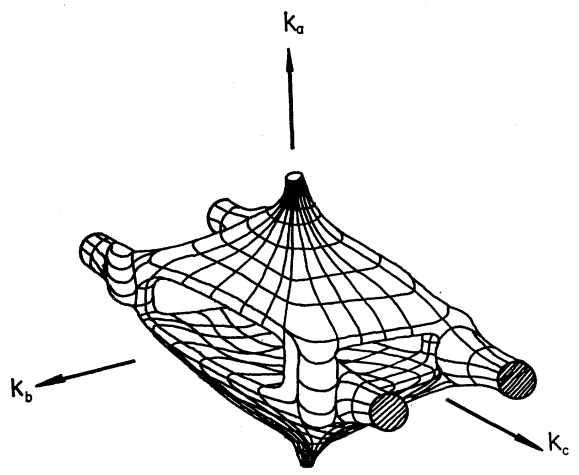

FIG. 12. Freely deformed single-OPW model: a proposed model of sixth-band hole surface having necessary restricted connectivity to explain present data.

B. Amplitude and Field Dependence of Induced Torque

The mean free path of electrons in gallium at 1.4°K has been shown to approximate the magnitude of the sample size and skin-depth parameter.[5] A self-consistent solution of the boundary-value problem of diffusing currents in the sample volume corresponds to a spacially-averaged field; the induced torque depends on a reduced value of field in a manner determined by the conductivity components. In angular regions over which these conductivity components are slowly varying, the modulation of the field dependence will remain approximately constant. Since the conductivity components are defined through integrals over the Fermi surface, it follows that a topology which varies slowly with crystalline angle is characterized by a slowly changing field dependence in the observed induced torque.

The induced-torque amplitude and field dependence due to the k_c trajectory have been shown to vary widely with field direction in the *ab* plane. The appearance of a relatively constant induced-torque amplitude, and nearly constant field dependence over the range $15°<\theta_{ab}<56°$ is indicative of a slowly varying topology. Conversely, the highly structured region $56°<\theta_{ab}<90°$ suggests a rapidly changing topology. Of particular interest are the two peaks near $(70.5\pm1)°$ and $(76.6\pm1)°$ which appear to be portions of a single large amplitude peak intersected by the sharp minimum at $(74.0\pm1)°$. The extreme alterations in amplitude and field dependence in this region are attributed to a gross alteration in Fermi-surface connectivity.

The pseudopotential model supports both an inner and outer k_c trajectory at each k_c-arm connection for all θ_{ab} except near $\theta_{ab}=0°$. The half-width of the null in

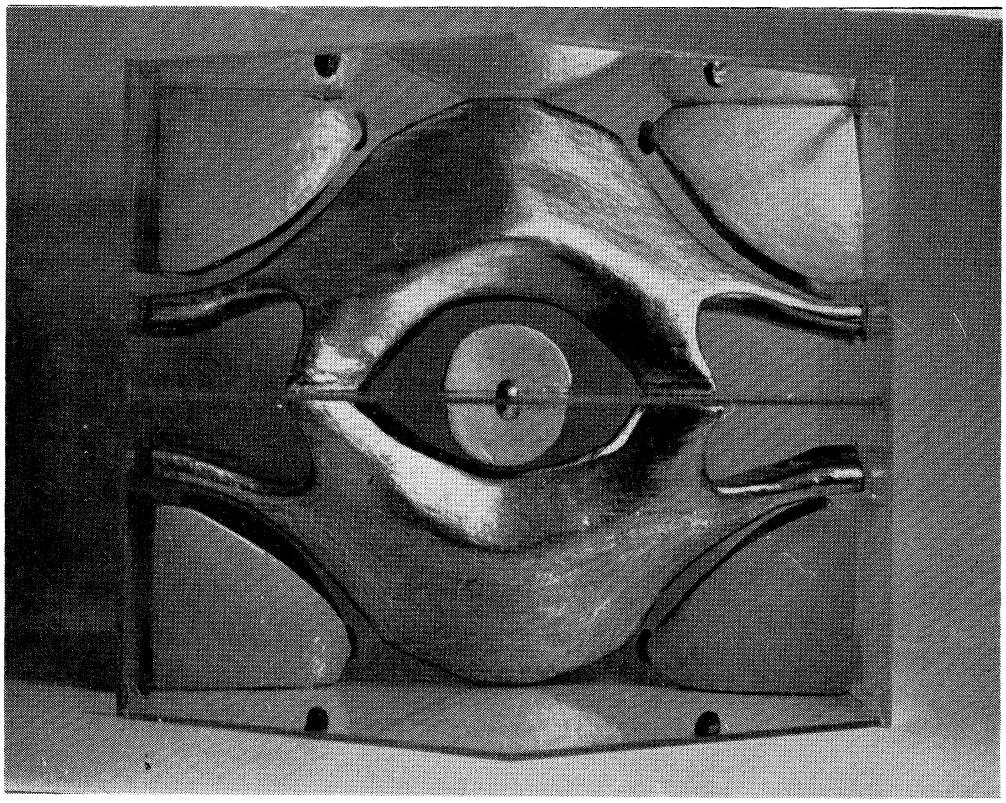

FIG. 13. Photograph of a model of the Fermi surface of gallium based on the pseudopotential calculations of W. A. Reed and constructed by R. Douglas. Pieces evident are the small crossed disk of eighth-band electrons, butterfly and saucer-shaped pieces of seventh-band electrons, the sixth-band monster, the small pancake of sixth-band holes between the arms of the monster, and the ellipsoid of sixth-band holes. There are also eighth-band electrons inside the butterfly and the cross-disk piece, and a small ellipsoid of fifth-band holes degenerate with the sixth-band holes at the top and bottom faces of the zone.

the vicinity of the a axis is predicted to be 13° on this model, in excellent agreement with observation. The rapid alterations in amplitude and field dependence for $56°<\theta_{ab}<90°$ are attributed to the influence of the k_a-neck connection. For a particular angular range on this model $\theta_{ab}=(69-72)°$ the outer trajectory group is interdicted by the k_a-neck connection. This interdiction reduces the open-orbit conductivity and is the source of the deep null observed in the induced-torque data at $(74.0\pm1)°$. In the vicinity of the k_a-neck connection the topology is rapidly varying; hence, the observed rapid variation in field dependence. In addition, the induced torque is expected to be large in the vicinity of the k_a-neck connection, through the large amplitude obtained in traversing the steeper sides of the convoluted cylinders. The linear shift of the peak from $\theta_{ab}=(68\pm1)°$ to $(61\pm1)°$ as field intensity is increased from 2 to 19 kOe is considered to be due to variation in the Fermi-surface parameters, affecting particular elements of the conductivity matrix.

The field dependence of the induced-torque amplitude for **B** within 0.1° of the b axis has been obtained for both a C and B crystal orientation. The former exhibits no evidence of magnetic breakdown (MB) in fields up to 20 kOe. The latter shows a decrease in open-orbit conductivity in fields above 8 kOe which could be due to MB. The latter was obtained for a large tilt angle (77°); the former tilt angle was approximately 2°. The evidence from the C sphere that no MB occurs in the k_c trajectory for **B** within 1/24° of the b axis in fields to 20 kOe is in agreement with the predictions of the pseudopotential model since breakdown could occur only to the seventh-band electron surface (butterfly) across a large energy gap (~0.15 eV). The observation at large tilt angles of apparent MB with $\mathbf{B}\|b$ axis raises several possibilities. Although the first experiment has been repeated to confirm its result, the possibility of error in this observation exists. Using the B-crystal orientation, the line shapes of the induced-torque amplitudes at higher fields are observed to broaden and to separate into two distinct peaks. The origin of this broadening and peak-splitting is not understood. Further, the inconsistency in the experimental evidence has not been resolved. It is possible that the model used to derive the induced-torque dependences is not valid for large tilt angle.

C. Tilt Dependence

The dependence of induced-torque amplitude on tilt angle β has been investigated for several separate orientations. The angular width of the k_c trajectory null at $\theta_{ab}=0°$ was defined by utilizing the irreducible wobble of the apparatus and by plotting the induced torque as a function of tilt angle using an A crystal. This dependence, however, was strongly modulated by the proximity of this null and cannot be readily compared with the predicted β dependence of Eq. (2). Using an E crystal and correlating the position of the a axis with the extrema of the tilt dependence, the second group was defined to be a k_a trajectory. The small amplitude of this orbit, however, lead to a poor determination of the detailed dependence. The most appropriate test of the predicted β dependence is provided by the B crystal data of Fig. 6. A least-squares fit to Eq. (1) is indicated by the solid line. The field dependence of the induced torque near the b axis has been shown to be approximately linear ($n=1$) in the absence of MB. If the extrinsic quadratic field dependence of Eq. (1) is reduced to linear, the least-squares fit yields

$$\rho_{yy}=1.0\times10^{-24}\text{ esu},\quad \rho_{zz}=2.8\times10^{-23}\text{ esu}.$$

The latter compared favorably with the value of approximate bulk resistivity at 1.4°K used earlier[9] ($\rho_0=5.5$ 10^{-23} esu).

It is to be emphasized that the β dependence has been obtained on the basis of a simple model calculation which is expected to be valid only for small tilt angles; the least-squares criterion forces agreement for general tilt angle. The excellent fit and the determination of reasonable resistivity parameters, however, are strong evidence for the usefulness of the model calculation.

D. Frequency Dependence

Experimentally, a linear dependence of induced-torque amplitude on frequency is found for copper,[24] cadmium,[19] and zinc.[21] For gallium, however, a strong deviation is observed, independent of relative peak amplitudes. Thus, the effect cannot be attributed to either a mechanical or electrical saturation effect. In addition, the peak widths and relative amplitudes are similar to those observed in cadmium, which shows no deviation from linearity. The origin of this effect is the similarity of the sample dimensions and skin-depth parameters ($\delta \gtrsim a$) at 1.4°K.

The observed frequency dependence shown in Fig. 11 has been fitted to the theoretical expressions derived by Landau and Lifshitz[25] to describe the torque induced in a sample of isotropic conductivity over the frequency range of interest. Since the sample used was a cylindrical A crystal, the equivalent radius for both the k_c and k_a trajectories was estimated (0.492 cm). The computed fits, adjusted for vertical scaling in accordance with estimates of the conductivity factors are presented in Fig. 11. Thus, the influence of the skin-effect region is observed for frequencies as low as 1.5×10^{-3} Hz in gallium.

VI. CONCLUSIONS

Using the induced-torque technique, the Fermi surface of gallium has been shown to support both k_a and k_c open trajectories over restricted angular ranges. In addition, the technique has been extended to treat anisotropic amplitude and field dependences in terms of topological alterations in the Fermi surface. This information has provided critical constraints for proposed models of the sixth-band hole surface, and has been shown consistent with that of recent pseudopotential calculations. A technique utilizing the dependence of torque amplitude on the tilt angle of the open trajectory out of the magnet sweep plane has been used with the irreducible wobble intrinsic in the apparatus to obtain alignments accurate to 0.1°. A nonlinear frequency dependence with frequencies as low as 1.5×10^{-3} Hz is shown to be due to the skin-depth region for samples used.

ACKNOWLEDGMENTS

We wish to thank Dr. W. A. Reed for several stimulating discussions and for furnishing us with calculations of the pseudopotential Fermi surface. We are also indebted to R. Douglas who constructed the Fermi-surface model shown in Fig. 13. The work was carried out with the financial support of the National Research Council of Canada. A scholarship (to J.R.C.) and the E.W.R. Steacie Fellowship (to W.R.D.) from N.R.C. are gratefully acknowledged.

[24] W. R. Datars, Phys. Letters 29A, 700 (1969).

[25] L. D. Landau and I. M. Lifshitz, *Electrodynamics of Continuous Media* (Pergamon Press, Inc., New York, 1960).

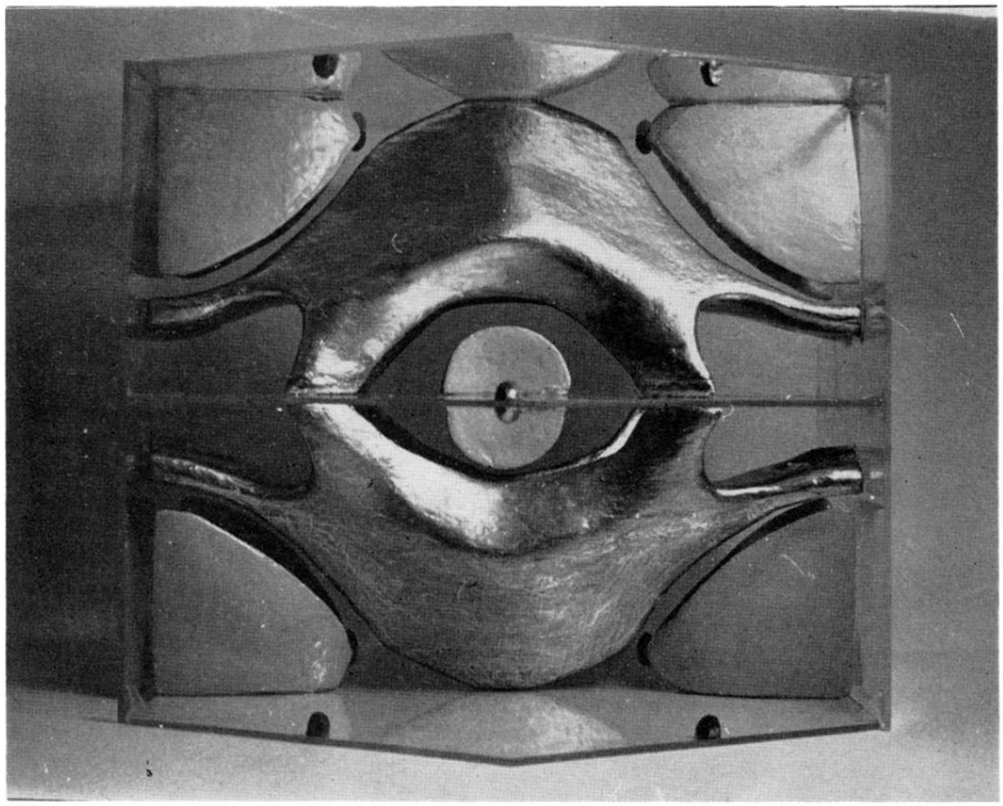

FIG. 13. Photograph of a model of the Fermi surface of gallium based on the pseudopotential calculations of W. A. Reed and con-constructed by R. Douglas. Pieces evident are the small crossed disk of eighth-band electrons, butterfly and saucer-shaped pieces of seventh-band electrons, the sixth-band monster, the small pancake of sixth-band holes between the arms of the monster, and the ellipsoid of sixth-band holes. There are also eighth-band electrons inside the butterfly and the cross-disk piece, and a small ellipsoid of fifth-band holes degenerate with the sixth-band holes at the top and bottom faces of the zone.